

pubs.acs.org/NanoLett Letter

Theory of Moire Magnetism in Twisted Bilayer !"RuCl₃

Muhammad Akram, Jesse Kapeghian, Jyotirish Das, Roser Valentí, Antia S. Botana,* and Onur Erten*



Cite This: Nano Lett. 2024, 24, 890-896



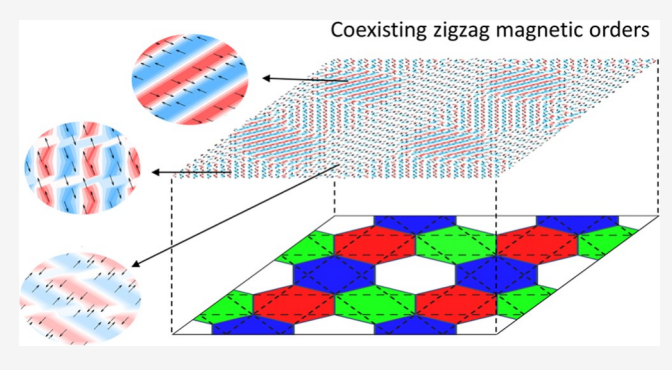
ACCESS |

Metrics & More

Article Recommendations

Supporting Information

ABSTRACT: Motivated by the recent developments in moire superlattices of van der Waals magnets and the desire to control the magnetic interactions of !-RuCl₃, here we present a comprehensive theory of the long-range ordered magnetic phases of twisted bilayer !-RuCl₃. Using a combination of first-principles calculations and atomistic simulations, we show that the stacking-dependent interlayer exchange gives rise to an array of magnetic phases that can be realized by controlling the twist angle. In particular, we discover a complex hexagonal domain structure in which multiple zigzag orders coexist. This multidomain order minimizes the interlayer energy while enduring the energy cost due to domain wall formation. Further, we show that quantum



fluctuations can be enhanced across the phase transitions. Our results indicate that magnetic frustration due to stacking-dependent interlayer exchange in moire superlattices can be exploited to tune quantum fluctuations and the magnetic ground state of !-RuCl₃.

KEYWORDS: 2D vdW magnets, !-RuCl₃, moire patterns, frustrated magnetism

!-RuCl2 is a van der Waals (vdW) magnet that has attracted a lot of attention in recent years as a promising candidate for a Kitaev quantum spin liquid (QSL). However, its zigzag antiferromagnetic (AFM) order below T_N " 7 K²⁻⁶ indicates deviations from the Kitaev model. The specific nature of these deviations has been theoretically and experimentally intensively scrutinized, with many works pointing to additional large anisotropic couplings beyond the Kitaev interaction and longrange exchange likely stabilizing magnetic order. 7-12 Under the application of an in-plane magnetic field, the zigzag order is suppressed, leading to a field-induced "disordered" phase, whose nature is presently still under intensive debate, especially due to initial reports of the observation of halfquantized thermal Hall conductivity. 13 This behavior would correspond to a chiral Kitaev spin liquid state. However, these results have not been corroborated so far. 14-16 Alternatively, there have been promising routes to investigate the emergence of novel phases beyond the zigzag AFM order by considering such approaches as chemical doping, 17 strain fields, 18-21 and graphene substrates.²²⁻²⁹ In the present work, we explore yet a new route to modify the magnetism in !-RuCl2, by exploring the properties of twisted bilayers of !-RuCl ,

Moire superlattices of van der Waals materials have surfaced as new tunable quantum platforms for the realization of emergent phases on every front, including graphene,³⁰ semiconductors,³¹ and superconductors.³² While moire engineering of electronic phases has been studied extensively, research in moire superlattices composed of magnetic materials is at its early stages. A range of novel noncoplanar phases have been predicted in moire vdW magnets,^{33–43} and some of these

phases have been observed experimentally. 44-46 Given that monolayers of !-RuCl₃ can be isolated by exfoliation methods 47,48 and heterostructures with other vdW materials such as graphene can be constructed, 25 moire engineering in !-RuCl₃ can be explored as a means to tune its magnetism.

Here, we study the long-range ordered magnetic phases of twisted bilayer !-RuCl3 by a combination of first-principles calculations and atomistic simulations. Our main results are as follows: (i) We obtain the stacking dependent interlayer exchange within the moire unit cell and show that the two layers are coupled antiferromagnetically for dilerent stacking orders. (ii) Among the three inequivalent ordering wave vectors $(q_i, i = 1, 2, 3)$ for the zigzag AFM order (see Figure 1e-g), the two layers spontaneously pick dilerent q's on each layer for large twist angles. This single-q phase (1q-1q) has no domain wall, but the interlayer exchange energy averages to almost zero. (iii) For small angles or large moire periodicity, the ground state incorporates all three of the q's in a complex domain structure (3q-3q). These domains resemble a hexagonal shape and minimize interlayer exchange. However, these domains are separated by domain walls that cost energy. (iv) Comparing the interlayer exchange and domain wall energy, we obtain an analytical formula for the transition

Received: October 23, 2023 Revised: January 7, 2024 Accepted: January 8, 2024 Published: January 10, 2024





Nano Letters pubs.acs.org/NanoLett Letter

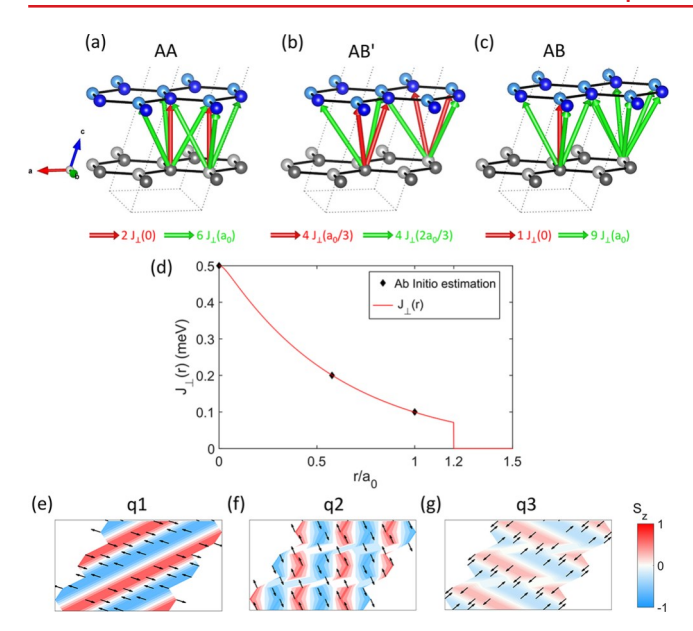


Figure 1. (a-c) Schematic representation of the three di!erent stackings used in our first-principles DFT calculations on bilayer !-RuCl₃ displaying the interlayer neighbors exchange couplings considered (for half a unit cell) as shown in eqs 4–6. (d) Continuous

interlayer exchange coupling function $J_{\perp}(r)=J_{\perp}(0)~{\rm e}^{-B\sqrt{c^2+r^2}/C}/{\rm e}^{-B}$ as a function of displacement r. Here, we use $J_{\infty}(0)=0.5~{\rm meV}$ obtained from our ab initio DFT estimation. (e–g) Spin textures for the zigzag AFM order for a 7 × 7 system. There are three inequivalent ordering wave vectors, $q_{1'}$ $q_{2'}$ and $q_{3'}$ that are related with C_3 symmetry.

between these two phases which agrees well with the atomistic simulations. (v) In the vicinity of the 1q-1q and 3q-3q phase boundary, we obtain an intermediate phase with two q's on each layer (2q-2q) that has both domain walls and finite interlayer exchange energy.

We start by introducing the spin Hamiltonian, which describes the magnetic properties of twisted bilayer !-RuCl₃. For simplicity we limit ourselves to a minimal set of exchange parameters, which have proven to provide a reasonable description of several experimental observations in !-RuCl₃:9

$$\mathcal{H} = \mathcal{H}_{intra}^{1} + \mathcal{H}_{intra}^{2} + \mathcal{H}_{inter}$$
 (1)

where $\mathcal{H}_{intra}^{1(2)}$ contains the intralayer exchange terms in layer 1 (2) and \mathcal{H}_{inter} contains the interlayer exchange:

$$\mathcal{H}_{intra} = \sum_{\langle ij \rangle_{\gamma}} [J_{1} \mathbf{S}_{i} \cdot \mathbf{S}_{j} + K S_{i}^{\gamma} S_{j}^{\gamma} + \Gamma(S_{i}^{\alpha} S_{j}^{\beta} + S_{j}^{\alpha} S_{i}^{\beta})] + J_{3} \sum_{\langle \langle \langle ij \rangle \rangle \rangle} \mathbf{S}_{i} \cdot \mathbf{S}_{j}$$
(2)

$$\mathcal{H}_{inter} = \sum_{\langle ij \rangle} J_{\perp}(r_{ij}) \mathbf{S}_{i}^{1} \cdot \mathbf{S}_{j}^{2}$$
(3)

where " = x, y, z type bonds on the honeycomb lattice. $J_{1(3)}$ is the (third) nearest-neighbor Heisenberg exchange; K and S are the Kitaev and the symmetric anisotropic exchange interaction terms. $J_{\%}(r_{ij})$ is the interlayer exchange coupling, and r_{ij} represents the interlayer displacement.

For the intralayer exchange parameters, we used K=-5 meV, \$=2.5 meV, $J_1=-0.5$ meV, and $J_3=0.5$ meV as obtained in ref 9. In order to determine the interlayer

exchange, we perform first-principles density functional theory (DFT) calculations for three di!erent bilayer stackings (AA, AB&, and AB) shown in Figure 1 (details on the *ab initio* DFT calculations are provided in the Supporting Information). For each stacking, we extract the energy di!erence ('E) between two spin configurations: ferromagnetic (FM), with FM planes coupled to FM out-of-plane, and antiferromagnetic (AFM), corresponding to FM planes coupled to AFM out-of-plane. Even though the magnetic ground state in RuCl₃ is zigzag-like, as mentioned above, we use the energy di!erence between these simpler spin configurations to obtain an estimate of the e!ective interlayer exchange. Importantly, for all stackings, we obtain a lower energy for an e!ective AFM interlayer coupling.

For the three stacking orders used, we construct an interlayer spin Hamiltonian in which the exchange coupling depends on the displacement, $J_{\%}(r_{ij})$, and we equate the energy dilerence from the *ab initio* DFT calculations ('E) to the corresponding elective interlayer spin Hamiltonian. For instance, the unit cell for the AA stacking used in the first-principles calculations has four interlayer bonds with $r_{ij} = 0$ and 12 bonds with $r_{ij} = a/(3)$ (see Figure 1a–c for a schematic picture of the interlayer bonds). In this manner, we obtain three equations for the three dilerent stacking patterns used.

$$4J_{\perp}(0) + 12J_{\perp}(a_0) = \Delta E_{AA}/2 = 3.2 \text{ meV}$$
 (4)

$$8J_1(a_0/3) + 8J_1(2a_0/3) = \Delta E_{AB'}/2 = 1.6 \text{ meV}$$
 (5)

$$2J_1(0) + 18J_1(a_0) = \Delta E_{AB}/2 = 2.8 \text{ meV}$$
 (6)

where $a_0 = a/(3)$ is the bond length on the honeycomb lattice. We implement a cuto! for the range of the exchange interaction, J(r = 2a/3)) 0, and solve eqs 4, 5, and 6, obtaining J(0) = 0.5 meV, $J(\alpha_0/(3)) = 0.2$ meV, and $J(\alpha_0) =$ 0.1 meV. Similar values of the interlayer exchange parameters have been reported in previous work. 49,50 To determine a continuous $J(r_{ij})$, we fit these values to an exponential decaying function, $J_{\perp}(r) = J_{\perp}(0) e^{-B\sqrt{C^2+r^2}/C}/e^{-B}$ (as shown in Figure 1d), with $\dot{B} = 0.04898$ and C = 0.02943 being the fitting parameters. Since the interlayer exchange is antiferromagnetic regardless of the stacking order (for both monoclinic and rhombohedral), we expect that our mapping scheme to an elective spin model is su"cient to demonstrate the elects of interlayer exchange in !-RuCl3. In contrast, if the sign of the interlayer exchange changes depending on the stacking order, more sophisticated methods involving moire maps of interlayer exchange can be necessary, as in the case of CrI₃^{37,42}

For a bilayer "untwisted" !-RuCl $_3$ with AA stacking order, the antiferromagnetic interlayer exchange is not frustrated, and the energy is minimized when both layers have the same single-q zigzag order. Due to the 3-fold rotational symmetry, there are three possible single-q patterns as shown in Figure 1e–g. On the contrary, for moire superlattices, the real space stacking within the moire unit cell changes as a function of displacement R. For small twist angles, the local stacking can by described by a translational shift, r(R) * $\#z \times R$ as shown in Figure 2a. Due to this varying shift, the nearest neighbor spins in two layers cannot be antiparallel throughout the moire unit cell when both layers have the same single-q order. To show this elect, we present in Figure 2b,c,d the projections of the nearest neighbor spins of layer-2 on the spins of layer-1

times the exponential decaying function $e^{-B\sqrt{C^2+r^2}}/C/e^{-B}$ used above for $J_{\%}$ for q_1 , q_2 , and q_3 , respectively. For 1q-1q zigzag

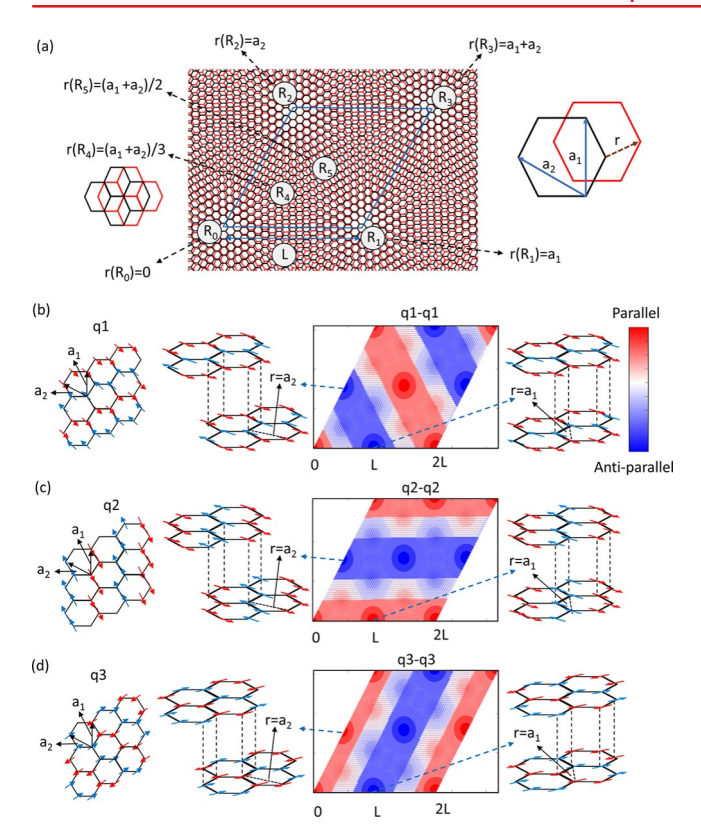


Figure 2. Moire pattern and projection of the nearest neighbor spins of layer-2 on the spins of layer-1 in twisted bilayer RuCl $_3$ (a) Moire pattern of a twisted bilayer system. For a small angle, the local stackings of the moire unit cell can be considered as the untwisted bilayer system with one layer shifted by displacement r. (b) q_1 zigzag order and the projection of first nearest neighbor spins of layer-2 on the spins of layer-1 times an exponential decaying function of in-plane displacement r with q_1 zigzag order in both layers of a 2 \times 2 moire unit cell (L " a/#). The red and blue colors represent parallel and antiparallel spins, respectively. (c and d) The same analysis as b for q_2 and q_3 , respectively.

order with q_1 on each layer, the spins are parallel at R_0 with a zero shift as shown in Figure 2b. At R_1 and R_2 , the translational shifts are a_1 and a_2 , respectively, and both of these shifts move a parallel spin to the location of an antiparallel spin. The whole pattern of varying parallel and antiparallel local stacking orders can be obtained in this way for the q_2 and q_3 orders as well. Based on the local translational shifts, the 1q-1q zigzag order in a 2 × 2 moire unit cell can be divided into three equal parts as shown in Figure 2b,c,d. In the one-third area, the spins are aligned parallel to each other, and this area is represented by red color, whereas in the second one-third area, they are arranged antiparallel (blue color). In the last one-third area, the spins are both parallel and antiparallel (white color). Therefore, the total interlayer exchange energy averages to zero. Even though this analysis is carried out when both layers have the same wave vector, it holds true for dilerent q_i 's on each layer as well.

However, the interlayer energy can be minimized if there are multiple-q zigzag patterns in each layer that are separated by domain walls. In Figure 2b–d, the white regions represent the areas where q_1 , q_2 , and q_3 orders cannot gain interlayer energy, respectively. These regions are combined in a single graph in Figure 3a that shows a schematic representation of constraints on the wave vectors that minimize the interlayer exchange

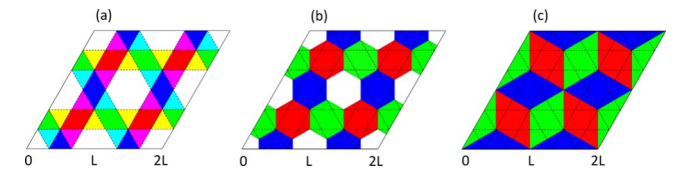


Figure 3. (a) Schematic representation of constraints on the wave vectors that minimize the interlayer exchange energy. Red, blue, and green diamonds represent regions where only q_1 , q_2 , and q_3 can gain interlayer energy, respectively. On the other hand, violet, yellow, and pink colors represent regions where q_1 , q_2 , and q_3 on their own cannot gain energy. White color represent regions where all the three q's can gain interlayer energy. (b,c) Two examples of multidomain structures that minimize the interlayer exchange energy. Red, blue, and green colors represent q_1 , q_2 , and q_3 zigzag orders, respectively. The white hexagons in b represent regions where any of the three q's is allowed.

energy. We implement the following color coding: the intersection of yellow and magenta bars is represented by red diamonds, where both \boldsymbol{q}_2 and \boldsymbol{q}_3 orders cannot gain energy. Therefore, the red diamonds display \boldsymbol{q}_1 order. Similarly, blue and green diamonds represent regions where only \boldsymbol{q}_2 and \boldsymbol{q}_3 can gain energy, respectively. The violet, yellow, and pink colors represent regions where only \boldsymbol{q}_1 , \boldsymbol{q}_2 , and \boldsymbol{q}_3 cannot gain energy. In the white region, any of the three wave vectors can gain energy. Applying these rules, we have constructed two examples of multidomain structures in Figure 3b and c. The white hexagons in Figure 3b can be filled with any one of the three \boldsymbol{q} orders. The domain structure in Figure 3c was predicted in ref 34 using a continuum model instead. Both of these configurations (b and c) fully minimize the interlayer energy and diler only by the domain wall length.

The competition between the domain wall and the interlayer energy leads to interesting phases as a function of the moire period (or twist angle) and interlayer coupling. We obtain the corresponding phase diagram by solving the Landau-Lifshitz-Gilbert (LLG) equation⁵¹ for both layers as shown in Figure 4a. For the interlayer exchange, we use the form derived from first-principles calculations, but we vary the overall amplitude, J (0). For a small moire period (or large twist angle), the ground state is in a(1q-1q) phase as shown in Figure 4b. In this phase, both layers have dilerent single-q zigzag patterns. These zigzag patterns are deformed from perfect order, leading to some gain in the interlayer energy. The degree of deformation increases with $J_{\%}$. For large moire periodicity (L) and large $J_{\%}$, we obtain the 3q-3q phase. In this phase, all three possible zigzag patterns are formed, as shown in Figure 4c. This phase is consistent with Figure 3b, and the shape of the zigzag patterns is hexagonal. One of the three q's occupies the white hexagons of Figure 3b, and it forms a larger domain of three hexagons connecting the opposite hexagons of the same q. This phase maximizes the interlayer energy, and the gain in interlayer energy in 2 \times 2 moire unit cells is E_{∞} " J_{∞} \times $N - J_{\%} 8(L/a_{0})^{2}/3$, where N is the number of sites and a_{n} is the bond length. On the other hand, the cost of domain wall energy formation is approximately E_{DW} " $40L\& \times 5.6623/$ (3 a_0 meV, where 40L& is the length of the domain walls and $L\& = L/(4 \cos(5/6))$ is the edge length of the hexagons (see Supporting Information for the derivation of E_{DW}). A critical moire period for the phase transition from $1q - \ddot{1}q$ to 3q - 3qcan be attained by equating $E_{\rm DW}$ and $E_{\rm w}$ leading to $L_{\rm crit} = (14.1562 \ {\rm meV/}J_{\rm w})a_{\rm 0}$. We find that the second candidate domain structure shown in Figure 3c has a longer domain wall

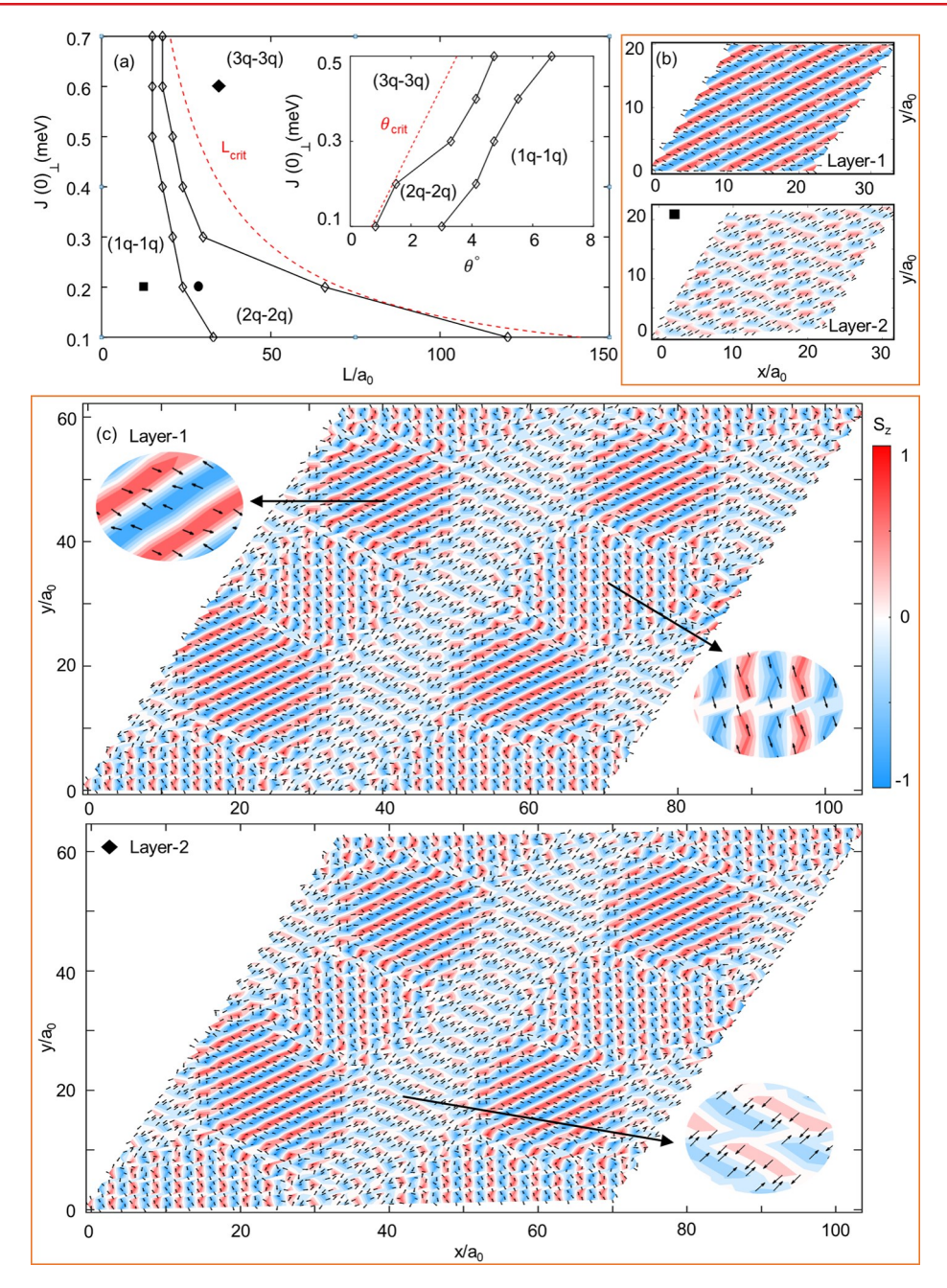


Figure 4. (a) Phase diagram of twisted bilayer I-RuCl as a function moire period L and J. The ab initio estimate is J (0) $\frac{1}{2}$ 0.5 meV. The inset shows the same phase diagram as a function twisted angle # and interlayer coupling J. Magnetization texture of (b) 1q-1q for L=12a and J (0) =0.2 meV and (c) 3q-3q for $L=36a_0$ and $J_{\%}(0)=0.6$ meV. Magnetization textures are shown for 2×2 moire unit cells.

length, and therefore, it is not preferred when compared to the hexagonal domain structure. The dashed line in Figure 4a represents the analytical estimate for the 1q-1q to 3q-3q phase transition. For intermediate moire periods, we obtain an intermediate 2q-2q phase as shown in Figure 5. In this phase, there are two kinds of zigzag patterns giving rise to a large fraction of interlayer energy. However, it is not possible to obtain a maximum interlayer energy from double zigzag patterns. On the contrary, such patterns have shorter domain wall length compared to 3q-3q phase. For small $J_{\%}$, the 2q-2q phase exists for a range of moire periods whereas for large $J_{\%}$ this phase exists only for a very short-range of small moire periods and the distinction between 1q-1q and 2q-2q phases is not evident.

The competition between a QSL state and zigzag AFM order seems to be crucial for the magnetism of $I\text{-RuCl}_3$. Our analysis shows that the moire interlayer exchange introduces a new type of magnetic frustration, weakening the zigzag AFM order. However, it is challenging to have conclusive remarks on how the interlayer exchange alects the QSL state, since the Kitaev model with additional \$ and Heisenberg terms is not exactly solvable. It is also not possible to perform exact diagonalization calculations for the twisted bilayer due to the large system size. However, recent mean-field theory calculations for bilayer and moire superlattices of Kitaev-type models $^{5\,2-54}$ suggest that the Kitaev spin liquid is stable up to a certain value of the interlayer exchange, and twisting does not have an additional impact on the QSL. Therefore, we can

Nano Letters pubs.acs.org/NanoLett Letter

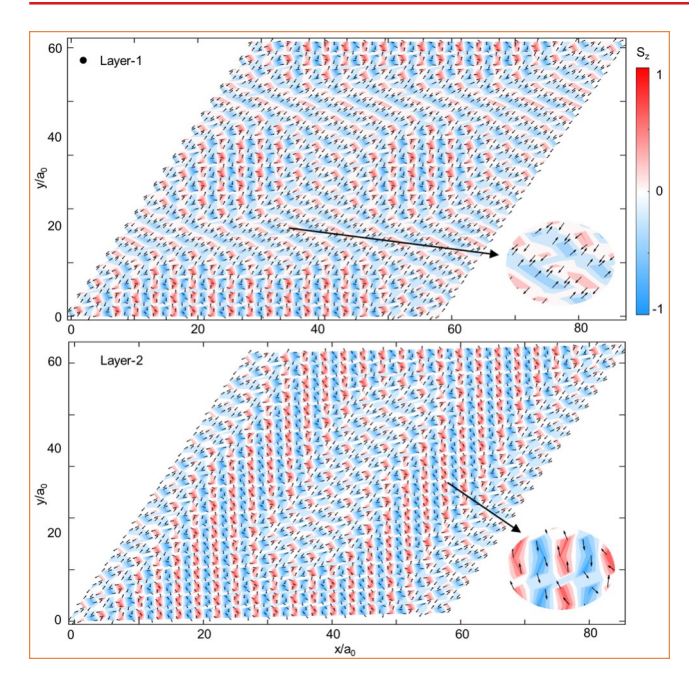


Figure 5. Magnetization texture of 2q-2q for $L=30a_0$ and $J_{\%}(0)=0.2$ meV. Magnetization texture is shown for 2×2 moire unit cells.

conclude that twisting has an overall negative impact on the zigzag order and therefore tilts the scale toward the QSL on the competition between these two phases.

In conclusion, we have shown that the interplay of the stacking-dependent interlayer exchange and twist angle can play an important role in determining the magnetic phases of l-RuCl $_3$. In particular, we demonstrate that the single-domain 1q-1q zigzag order can be taken over by multi-q patterns in order to minimize the interlayer exchange energy. These phases appear at small twist angles and can be used as a new route to introduce additional frustration and tune the magnetic phases in l-RuCl $_3$. Interesting future directions include estimating the magnon spectrum in multi-q orders and incorporating substrate elects.

* ASSOCIATED CONTENT * Supporting Information

The Supporting Information is available free of charge at https://pubs.acs.org/doi/10.1021/acs.nanolett.3c04084.

Structural parameters, estimation of domain wall energy cost, details of the atomistic simulations (PDF)

AUTHOR INFORMATION Corresponding Authors

Antia S. Botana – Department of Physics, Arizona State University, Tempe, Arizona 85287, United States; Email: antia.botana@asu.edu

Onur Erten – Department of Physics, Arizona State
University, Tempe, Arizona 85287, United States;
orcid.org/0000-0002-1944-239X; Email: onur.erten@asu.edu

Authors

Muhammad Akram – Department of Physics, Arizona State University, Tempe, Arizona 85287, United States; Department of Physics, Balochistan University of Information Technology, Engineering and Management Sciences (BUITEMS), Quetta 87300, Pakistan

Jesse Kapeghian – Department of Physics, Arizona State University, Tempe, Arizona 85287, United States

Jyotirish Das – Department of Physics, Arizona State University, Tempe, Arizona 85287, United States

Roser Valentí – Institut fur Theoretische Physik, Goethe-Universität Frankfurt, 60438 Frankfurt am Main, Germany

Complete contact information is available at: https://pubs.acs.org/10.1021/acs.nanolett.3c04084

Author Contributions

M.A. and J.D. performed the atomistic simulations. J.K. performed the first-principles calculations. A.B. and O.E. conceptualized the research and analyzed the results. All authors contributed to writing the manuscript.

Note

The authors declare no competing financial interest.

ACKNOWLEDGMENTS

We thank Arun Paramekanti for fruitful discussions. O.E. and A.B. acknowledge support from National Science Foundation Award No. DMR 2206987. M.A. acknowledges support from National Science Foundation Awards No. DMR 2234352. We acknowledge the ASU Research Computing Center for HPC resources. R.V. acknowledges the DFG (German Research Foundation) for funding through the research unit QUAST FOR 5249 (project ID: 449872909; project P4), and her research was supported in part by the National Science Foundation under grant nos. NSF PHY-1748958 and PHY-2309135.

REFERENCES

- (1) Kitaev, A. Anyons in an exactly solved model and beyond. *Ann. Phys.* 2006, *321*, 2–111.
- (2) Banerjee, A.; Yan, J.; Knolle, J.; Bridges, C. A.; Stone, M. B.; Lumsden, M. D.; Mandrus, D. G.; Tennant, D. A.; Moessner, R.; Nagler, S. E. Neutron scattering in the proximate quantum spin liquid ! RuCl₂. Science 2017, 356, 1055–1059.
- (3) Banerjee, A.; et al. Proximate Kitaev quantum spin liquid behaviour in a honeycomb magnet. *Nat. Mater.* 2016, 15, 733–740. (4) Cao, H. B.; Banerjee, A.; Yan, J.-Q.; Bridges, C. A.; Lumsden, M.
- D.; Mandrus, D. G.; Tennant, D. A.; Chakoumakos, B. C.; Nagler, S. E. Low-temperature crystal and magnetic structure of ! RuCl₃. *Phys. Rev. B* 2016, *93*, 134423.
- (5) Plumb, K. W.; Clancy, J. P.; Sandilands, L. J.; Shankar, V. V.; Hu, Y. F.; Burch, K. S.; Kee, H.-Y.; Kim, Y.-J. !-RuCl ; A spin-orbit assisted Mott insulator on a honeycomb lattice. *Phys. Rev. B* 2014, *90*, No. 041112.
- (6) Johnson, R. D.; Williams, S.; Haghighirad, A.; Singleton, J.; Zapf, V.; Manuel, P.; Mazin, I.; Li, Y.; Jeschke, H. O.; Valentí, R.; Coldea, R. Monoclinic crystal structure of *!* RuCl 3 and the zigzag antiferromagnetic ground state. *Phys. Rev. B* 2015, *92*, 235119.
- (7) Rau, J. G.; Lee, E. K.-H.; Kee, H.-Y. Generic Spin Model for the Honeycomb Iridates beyond the Kitaev Limit. *Phys. Rev. Lett.* 2014, 112, No. 077204.
- (8) Winter, S. M.; Li, Y.; Jeschke, H. O.; Valentí, R. Challenges in design of Kitaev materials: Magnetic interactions from competing energy scales. *Phys. Rev. B* 2016, *93*, 214431.
- (9) Winter, S. M.; Riedl, K.; Maksimov, P. A.; Chernyshev, A. L.; Honecker, A.; Valentí, R. Breakdown of magnons in a strongly spinorbital coupled magnet. *Nat. Commun.* 2017, *8*, 1152.
- (10) Winter, S. M.; Tsirlin, A. A.; Daghofer, M.; van den Brink, J.; Singh, Y.; Gegenwart, P.; Valentí, R. Models and materials for

- generalized Kitaev magnetism. J. Phys.: Condens. Matter 2017, 29, 493002
- (11) Maksimov, P. A.; Chernyshev, A. L. Rethinking ! RuCl₃ *Phys. Rev. Res.* 2020, *2*, No. 033011.
- (12) Rousochatzakis, I.; Perkins, N. B.; Luo, Q.; Kee, H.-Y. Beyond Kitaev physics in strong spin-orbit coupled magnets. *arXiv* 2023, arXiv:2308.01943. https://arxiv.org/abs/2308.01943 (accessed August 3, 2023).
- (13) Yokoi, T.; Ma, S.; Kasahara, Y.; Kasahara, S.; Shibauchi, T.; Kurita, N.; Tanaka, H.; Nasu, J.; Motome, Y.; Hickey, C.; Trebst, S.; Matsuda, Y. Half-integer quantized anomalous thermal Hall effect in the Kitaev material candidate ! RuCl₃. Science 2021, 373, 568–572.
- (14) Lefrancois, E.; Grissonnanche, G.; Baglo, J.; Lampen-Kelley, P.; Yan, J.-Q.; Balz, C.; Mandrus, D.; Nagler, S. E.; Kim, S.; Kim, Y.-J.; Doiron-Leyraud, N.; Taillefer, L. Evidence of a Phonon Hall Effect in the Kitaev Spin Liquid Candidate *!*-RuCl 3. *Physical Review X* 2022, 12. No. 021025.
- (15) Bruin, J. A. N.; Claus, R. R.; Matsumoto, Y.; Kurita, N.; Tanaka, H.; Takagi, H. Robustness of the thermal Hall effect close to half-quantization in *!*-RuCl3. *Nat. Phys.* 2022. *18*, 401–405.
- (16) Czajka, P.; Gao, T.; Hirschberger, M.; Lampen-Kelley, P.; Banerjee, A.; Quirk, N.; Mandrus, D. G.; Nagler, S. E.; Ong, N. P. Planar thermal Hall effect of topological bosons in the Kitaev magnet *!*-RuCl3. *Nat. Mater.* 2023, 22, 36–41.
- (17) Bastien, G.; Roslova, M.; Haghighi, M.; Mehlawat, K.; Hunger, J.; Isaeva, A.; Doert, T.; Vojta, M.; Buchner, B.; Wolter, A. Spin-glass state and reversed magnetic anisotropy induced by Cr doping in the Kitaev magnet *!* RuCl 3. *Phys. Rev. B* 2019, *99*, 214410.
- (18) Bastien, G.; Garbarino, G.; Yadav, R.; Martinez-Casado, F. J.; Beltran Rodriguez, R.; Stahl, Q.; Kusch, M.; Limandri, S. P.; Ray, R.; Lampen-Kelley, P.; Mandrus, D. G.; Nagler, S. E.; Roslova, M.; Isaeva, A.; Doert, T.; Hozoi, L.; Wolter, A. U. B.; Buchner, B.; Geck, J.; van den Brink, J. Pressure-induced dimerization and valence bond crystal formation in the Kitaev-Heisenberg magnet !-RuCl 3. *Phys. Rev. B* 2018, *97*, 241108.
- (19) Bachus, S.; Kaib, D. A.; Tokiwa, Y.; Jesche, A.; Tsurkan, V.; Loidl, A.; Winter, S. M.; Tsirlin, A. A.; Valenti, R.; Gegenwart, P. Thermodynamic Perspective on Field-Induced Behavior of *!* RuCl 3. *Phys. Rev. Lett.* 2020, *125*, No. 097203.
- (20) Kocsis, V.; Kaib, D. A. S.; Riedl, K.; Gass, S.; Lampen-Kelley, P.; Mandrus, D. G.; Nagler, S. E.; Perez, N.; Nielsch, K.; Buchner, B.; Wolter, A. U. B.; Valenti, R. Magnetoelastic coupling anisotropy in the Kitaev material *!*-RuCl3. *Phys. Rev. B* 2022, *105*, No. 094410.
- (21) Kaib, D. A.; Biswas, S.; Riedl, K.; Winter, S. M.; Valentí, R. Magnetoelastic coupling and effects of uniaxial strain in *!*-RuCl3 from first principles. *Phys. Rev. B* 2021, *103*, L140402.
- (22) Mashhadi, S.; Kim, Y.; Kim, J.; Weber, D.; Taniguchi, T.; Watanabe, K.; Park, N.; Lotsch, B.; Smet, J. H.; Burghard, M.; Kern, K. Spin-split band hybridization in graphene proximitized with *!*-RuCl3 nanosheets. *Nano Lett.* 2019, *19*, 4659–4665.
- (23) Zhou, B.; Balgley, J.; Lampen-Kelley, P.; Yan, J.-Q.; Mandrus, D. G.; Henriksen, E. A. Evidence for charge transfer and proximate magnetism in graphene–! RuCl 3 heterostructures. *Phys. Rev. B* 2019, *100*, 165426.
- (24) Biswas, S.; Li, Y.; Winter, S. M.; Knolle, J.; Valentí, R. Electronic Properties of *!* RuCl 3 in proximity to graphene. *Phys. Rev. Lett.* 2019, *123*, 237201.
- (25) Rizzo, D. J.; et al. Charge-Transfer Plasmon Polaritons at Graphene/! -RuCl3 Interfaces. *Nano Lett.* 2020, *20*, 8438–8445.
- (26) Gerber, E.; Yao, Y.; Arias, T. A.; Kim, E.-A. Ab Initio Mismatched Interface Theory of Graphene on *!* RuCl 3: Doping and Magnetism. *Phys. Rev. Lett.* 2020, *124*, 106804.
- (27) Leeb, V.; Polyudov, K.; Mashhadi, S.; Biswas, S.; Valentí, R.; Burghard, M.; Knolle, J. Anomalous quantum oscillations in a heterostructure of graphene on a proximate quantum spin liquid. *Phys. Rev. Lett.* 2021, *126*, No. 097201.
- (28) Balgley, J.; Butler, J.; Biswas, S.; Ge, Z.; Lagasse, S.; Taniguchi, T.; Watanabe, K.; Cothrine, M.; Mandrus, D. G.; Velasco, J.; Valenti,

- R.; Henriksen, E. A. others Ultrasharp Lateral p-n Junctions in Modulation-Doped Graphene. *Nano Lett.* 2022, 22, 4124–4130.
- (29) Shi, J.; MacDonald, A. Magnetic states of graphene proximitized Kitaev materials. *Phys. Rev. B* 2023, *108*, No. 064401.
- (30) Cao, Y.; Fatemi, V.; Fang, S.; Watanabe, K.; Taniguchi, T.; Kaxiras, E.; Jarillo-Herrero, P. Unconventional superconductivity in magic-angle graphene superlattices. *Nature* 2018, *556*, 43–50.
- (31) Devakul, T.; Crépel, V.; Zhang, Y.; Fu, L. Magic in twisted transition metal dichalcogenide bilayers. *Nat. Commun.* 2021, *12*, 6730.
- (32) Zhao, S. Y. F.; Poccia, N.; Cui, X.; Volkov, P. A.; Yoo, H.; Engelke, R.; Ronen, Y.; Zhong, R.; Gu, G.; Plugge, S.; Tummuru, T.; Franz, M.; Pixley, J. H.; Kim, P. Emergent Interfacial Superconductivity between Twisted Cuprate Superconductors. *arXiv* 2021, arXiv:2108.13455. https://arxiv.org/abs/2108.13455 (accessed August 30, 2021).
- (33) Tong, Q.; Liu, F.; Xiao, J.; Yao, W. Skyrmions in the moire of van der Waals 2D Magnets. *Nano Lett.* 2018, 18, 7194–7199.
- (34) Hejazi, K.; Luo, Z.-X.; Balents, L. Noncollinear phases in moire magnets. *Proc. Natl. Acad. Sci. U. S. A.* 2020, *117*, 10721–10726.
- (35) Hejazi, K.; Luo, Z.-X.; Balents, L. Heterobilayer moire magnets: Moire skyrmions and commensurate-incommensurate transitions. *Phys. Rev. B* 2021, *104*, L100406.
- (36) Akram, M.; Erten, O. Skyrmions in twisted van der Waals magnets. *Phys. Rev. B* 2021, *103*, L140406.
- (37) Akram, M.; LaBollita, H.; Dey, D.; Kapeghian, J.; Erten, O.; Botana, A. S. Moire Skyrmions and Chiral Magnetic Phases in Twisted CrX3 (X = I, Br, and CI) Bilayers. *Nano Lett.* 2021, *21*, 6633–6639.
- (38) Xiao, F.; Chen, K.; Tong, Q. Magnetization textures in twisted bilayer CrX₃(. *Phys. Rev. Research* 2021, 3, No. 013027.
- (39) Xiao, F.; Chen, K.; Tong, Q. Magnetization textures in twisted bilayer CrX₃(X = Br, I). *Phys. Rev. Res.* 2021, *3*, No. 013027.
- (40) Ghader, D.; Jabakhanji, B.; Stroppa, A. Whirling interlayer fields as a source of stable topological order in moire CrI3. *Communications Physics* 2022, *5*, 192.
- (41) Zheng, F. Magnetic Skyrmion Lattices in a Novel 2D-Twisted Bilayer Magnet. *Adv. Funct. Mater.* 2023, *33*, 2206923.
- (42) Kim, K.-M.; Kiem, D. H.; Bednik, G.; Han, M. J.; Park, M. J. Ab Initio Spin Hamiltonian and Topological Noncentrosymmetric Magnetism in Twisted Bilayer Crl3. *Nano Lett.* 2023, *23*, 6088–6094.
- (43) Fumega, A. O.; Lado, J. L. Moire-driven multiferroic order in twisted CrCl3, CrBr3 and Crl3 bilayers. *2D Materials* 2023, *10*, No. 025026.
- (44) Xu, Y.; Ray, A.; Shao, Y.-T.; Jiang, S.; Lee, K.; Weber, D.; Goldberger, J. E.; Watanabe, K.; Taniguchi, T.; Muller, D. A.; Mak, K. F.; Shan, J. Coexisting ferromagnetic-antiferromagnetic state in twisted bilayer Crl3. *Nature Nanotechnol.* 2022, *17*, 143–147.
- (45) Song, T.; Sun, Q.-C.; Anderson, E.; Wang, C.; Qian, J.; Taniguchi, T.; Watanabe, K.; McGuire, M. A.; Stöhr, R.; Xiao, D.; Cao, T.; Wrachtrup, J.; Xu, X. Direct visualization of magnetic domains and moire magnetism in twisted 2D magnets. *Science* 2021, 374, 1140–1144.
- (46) Xie, H.; Luo, X.; Ye, Z.; Sun, Z.; Ye, G.; Sung, S.; Ge, H.; Yan, S.; Fu, Y.; Tian, S.; Lei, H.; Sun, K.; Hovden, R.; He, R.; Zhao, L. Evidence of non-collinear spin texture in magnetic moire superlattices. *Nat. Phys.* 2023, *19*, 1150–1155.
- (47) Lee, J.-H.; Choi, Y.; Do, S.-H.; Kim, B. H.; Seong, M.-J.; Choi, K.-Y. Multiple spin-orbit excitons in *!*-RuCl3 from bulk to atomically thin layers. *npj Quantum Materials* 2021, *6*, 43.
- (48) Yang, B.; et al. Magnetic anisotropy reversal driven by structural symmetry-breaking in monolayer *!*-RuCl3. *Nat. Mater.* 2023, *22*, 50–57.
- (49) Janssen, L.; Koch, S.; Vojta, M. Magnon dispersion and dynamic spin response in three-dimensional spin models for *!* RuCl³. *Phys. Rev. B* 2020, *101*, 174444.
- (50) Balz, C.; Janssen, L.; Lampen-Kelley, P.; Banerjee, A.; Liu, Y. H.; Yan, J.-Q.; Mandrus, D. G.; Vojta, M.; Nagler, S. E. Field-induced

intermediate ordered phase and anisotropic interlayer interactions in ! – RuCl $_3$. *Phys. Rev. B* 2021, *103*, 174417.

- (51) Gilbert, T. L. A phenomenological theory of damping in ferromagnetic materials. *IEEE Trans. Magn.* 2004, *40*, 3443–3449.
- (52) Seifert, U. F. P.; Gritsch, J.; Wagner, E.; Joshi, D. G.; Brenig, W.; Vojta, M.; Schmidt, K. P. Bilayer Kitaev models: Phase diagrams and novel phases. *Phys. Rev. B* 2018, *98*, 155101.
- (53) Haskell, S.; Principi, A. Emergent hypermagic manifold in twisted Kitaev bilayers. *Phys. Rev. B* 2022, *106*, L161404.
- (54) Vijayvargia, A.; Seifert, U. F. P.; Erten, O. Topological and magnetic phase transitions in the bilayer Kitaev-Ising model. *arXiv* 2023, arXiv:2311.06245. https://arxiv.org/abs/2311.06245 (accessed Nov 10, 2023).



pubs.acs.org/NanoLett Addition/Correction

Correction to "Theory of Moire Magnetism in Twisted Bilayer !"RuCl₃"

Muhammad Akram, Jesse Kapeghian, Jyotirish Das, Roser Valentí, Antia S. Botana,* and Onur Erten* *Nano Lett.* 2024, *24* (3), 890–896. DOI: 10.1021/acs.nanolett.3c04084



Cite This: https://doi.org/10.1021/acs.nanolett.4c01783



ACCESS

Metrics & More

Article Recommendations

e correct the Acknowledgments Section as follows: OE and AB acknowledge support from National Science Foundation Award No. DMR-2206987. MA acknowledges support from National Science Foundation Award No. DMR-2234352.

